Research Article | Vol. 25, No. 26 | 25 Dec 2017 | OPTICS EXPRESS 33134
Optics EXPRESS

Femtosecond laser-colorized indium-tin-oxide films for blue light attenuation and image screening

YA-HSIN TSENG, HUNG YANG, AND CHIH-WEI LUO*

Department of Electrophysics, National Chiao Tung University, Hsinchu 300, Taiwan
**cwluo@mail.nctu.edu.tw*

Abstract: Laser-colorized indium-tin-oxide (ITO) films are fabricated using femtosecond laser processing. By varying the laser fluences, nanostructures with cotton, brick and ripple forms are generated on the surface of ITO films, which produces cyan, yellow and orange colors. The fluence-dependent nanostructures on the surface of ITO films also significantly attenuates blue light so these materials are suited to eye protection and the screening of images behind ITO films for information security.

OCIS codes: (330.0330) Vision, color, and visual optics; (320.7130) Ultrafast processes in condensed matter, including semiconductors; (220.4241) Nanostructure fabrication; (190.4400) Nonlinear optics, materials.

References and links

1. J. Eichstadt, G. R. B. E. Romer, and A. J. H. Veld, "Towards friction control using laser-induced periodic surface structures," in *Proceedings of the Sixth International WLT Conference on Lasers in Manufacturing* (Munich, 2011), pp. 7–15.
2. A. Y. Vorobyev and C. Guo, "Multifunctional surfaces produced by femtosecond laser pulses," J. Appl. Phys. **117**(3), 033103 (2015).
3. C. Wang, H. I. Wang, W. T. Tang, C. W. Luo, T. Kobayashi, and J. Leu, "Superior local conductivity in self-organized nanodots on indium-tin-oxide films induced by femtosecond laser pulses," Opt. Express **19**(24), 24286–24297 (2011).
4. M. H. Chen, Y. H. Tseng, Y. P. Chao, S. Y. Tseng, Z. R. Lin, H. H. Chu, J. K. Chang, and C. W. Luo, "Effects on organic photovoltaics using femtosecond-laser-treated indium tin oxides," ACS Appl. Mater. Interfaces **8**(38), 24989–24993 (2016).
5. C. Wang, H. I. Wang, C. W. Luo, and J. Leu, "Anisotropic optical transmission of femtosecond laser induced periodic surface nanostructures on indium-tin-oxide films," Appl. Phys. Lett. **101**(10), 101911 (2012).
6. A. Y. Vorobyev and C. L. Guo, "Metallic light absorbers produced by femtosecond laser pulses," Adv. Mech. Eng. **2**, 452749 (2010).
7. A. Y. Vorobyev and C. Guo, "Enhanced absorptance of gold following multipulse femtosecond laser ablation," Phys. Rev. B **72**(19), 195422 (2005).
8. A. Y. Vorobyev and C. L. Guoa, "Colorizing metals with femtosecond laser pulses," Appl. Phys. Lett. **92**(4), 041914 (2008).
9. J. Bonse, S. Hohm, S. V. Kirner, A. Rosenfeld, and J. Kruger, "Laser-induced periodic surface structures-a scientific evergreen," IEEE J. Sel. Top. Quantum Electron. **23**(3), 9000615 (2017).
10. X. Zhu, W. Yan, U. Levy, N. A. Mortensen, and A. Kristensen, "Resonant laser printing of structural colors on high-index dielectric metasurfaces," Sci. Adv. **3**(5), e1602487 (2017).
11. A. Masamichi, K. Hideki, K. Hiroaki, S. Yasuyuki, I. Takafumi, and T. Yoshiro, "Pressure-sensitive touch panel based on piezoelectric poly(L-lactic acid) film," Jpn. J. Appl. Phys. **52**(9S1), 09KD17 (2013).
12. C. W. Cheng, C. Y. Lin, W. C. Shen, Y. J. Lee, and J. S. Chen, "Patterning crystalline indium tin oxide by high repetition rate femtosecond laser-induced crystallization," Thin Solid Films **518**(23), 7138–7142 (2010).
13. C. W. Cheng and C. Y. Lin, "High precision patterning of ITO using femtosecond laser annealing process," Appl. Surf. Sci. **314**, 215–220 (2014).
14. Anar Foundation, "Only for Children," https://www.youtube.com/watch?v=6zoCDyQSH0o
15. J. Bonse, A. Rosenfeld, and J. Krüger, "On the role of surface plasmon polaritons in the formation of laser-induced periodic surface structures upon irradiation of silicon by femtosecond-laser pulses," J. Appl. Phys. **106**(10), 104910 (2009).
16. D. Dufft, A. Rosenfeld, S. K. Das, R. Grunwald, and J. Bonse, "Femtosecond laser-induced periodic surface structures revisited: A comparative study on ZnO," J. Appl. Phys. **105**(3), 034908 (2009).
17. J. E. Sipe, J. F. Young, J. S. Preston, and H. M. van Driel, "Laser-induced periodic surface structure. I. Theory," Phys. Rev. B **27**(2), 1141–1154 (1983).

#310139 https://doi.org/10.1364/OE.25.033134
Journal © 2017 Received 27 Oct 2017; revised 13 Dec 2017; accepted 13 Dec 2017; published 20 Dec 2017

Optics EXPRESS

18. S. Ray, R. Banerjee, N. Basu, A. K. Batabyal, and A. K. Barua, "Properties of tin doped indium oxide thin films prepared by magnetron sputtering," J. Appl. Phys. **54**(6), 3497–3501 (1983).
19. T. A. F. König, P. A. Ledin, J. Kerszulis, M. A. Mahmoud, M. A. El-Sayed, J. R. Reynolds, and V. V. Tsukruk, "Electrically tunable plasmonic behavior of nanocube-polymer nanomaterials induced by a redox-active electrochromic polymer," ACS Nano **8**(6), 6182–6192 (2014).
20. I. Jaadane, P. Boulenguez, S. Chahory, S. Carré, M. Savoldelli, L. Jonet, F. Behar-Cohen, C. Martinsons, and A. Torriglia, "Retinal damage induced by commercial light emitting diodes (LEDs)," Free Radic. Biol. Med. **84**, 373–384 (2015).
21. A. K. Kulkarni, K. H. Schulz, T. S. Lim, and M. Khan, "Dependence of the sheet resistance of indium-tin-oxide thin films on grain size and grain orientation determined from X-ray diffraction techniques," Thin Solid Films **345**(2), 273–277 (1999).

1. Introduction

The need for ink- and toxin-free painting means that laser colorization using laser-induced periodic surface structures (LIPSSs) [1–7] is important because it is environmentally friendly. Recently, LIPSSs have been observed on various materials and this type of surface structures also modifies some physical properties, such as the friction [1], the hydrophobicity/ hydrophilicity [2], the conductivity [3–5] and the absorptance [2,6,7]. Laser-colorized materials are realized by controlling the morphology. For example, a variety of colors for different metals (e.g., aluminum [8], stainless steel [9], etc.) and semiconductors (e.g., Ge [10]) was demonstrated using a femtosecond laser processing technique. However, to the authors' best knowledge, there has been no attempt to colorize transparent conducting materials using femtosecond laser processing. This study shows that the color of indium-tin-oxide (ITO) films can be easily controlled using femtosecond laser processing.

ITO is both transparent and conducting and is an important material for industrial applications in solar cells [4] and touch panels [11]. There have been many attempts to enhance the transparency and reduce the resistivity via femtosecond laser-induced crystallization [12]. Precisely selective crystallization using laser annealing [13] allows areas to be patterned and the line width of electrodes in touch panels to be reduced [11]. Touch panels are indispensable devices for work, communication, and entertainment. Eye protection and the preservation of personal privacy is important issue for long-term usage.

This study fabricates various nanostructures on the surface of ITO films by using femtosecond laser processing to modify their optical properties. The femtosecond laser-colorized ITO films are highly transparent and have potential applications for blue light attenuation to protect eyes and in image screening to secure information [14].

2. Experiments

ITO films with a thickness of 80 nm for this study were coated on 1.1-mm-thick glass. The ITO films were mounted on an xyz-stage and irradiated at room temperature and ambient pressure using a commercial Ti:sapphire amplifier (Solstice Ace, Spectra-Physics) with a central wavelength of 800 nm, a pulse duration of 35 fs and a repetition rate of 2 kHz. A cylindrical lens (f = 40 mm) was used to focus the laser beam into a line spot with a length of 4.6 mm and a width of 21 μm. The scanning speed was approximately 160 μm/s.

The morphology of the ITO films was observed using high resolution field emission scanning electron microscopy (SEM, JEOL). A spectrometer (U3310, Hitachi) with both deuterium and tungsten iodide lamps (allowing for a scanning range from 190 nm to 900 nm with a resolution of 0.3 nm) was used to determine the relationship between the reflectance/transmittance spectra and the colors of femtosecond laser-colorized ITO films.

3. Results and discussions

SEM images of the surface morphology of an untreated ITO film and five laser-annealed ITO films are shown in Fig. 1 (all of the experimental conditions used in this study are summarized in Table 1). For sample UDL-1 in Fig. 1(b), a densely cotton-like structure is observed on the surface with a fluence of 646 mJ/cm^2. Decreasing the laser fluence causes the

Optics EXPRESS

cotton-like structure to gradually disappear and a brick-like structure emerges. At a low fluence of 60 mJ/cm^2, a regular ripple structure that is formed by nano-bricks is clearly observed on the surface, as shown in Fig. 1(f). All of the ripples (formed by nano-bricks) in Figs. 1(c)–1(f) were fabricated by scanning a laser spot along the y-axis, which is parallel to the polarization of laser beam. The spatial period along the y-axis is much smaller than the wavelength of the radiation, which is the so-called high spatial frequency LIPSS (HSFL). HSFLs are usually generated on transparent materials using hundreds to thousands of ultra-short laser pulses [15] perpendicular to the direction of laser polarization with a fluence that is below the damage threshold of materials [16]. In this study, all of ITO films were irradiated by about 260 pulses at a single point, depending on the scanning speed of ~12.5 pulses/μm and the 21-μm width of laser line spot. The HSFLs can be successfully generated on the surface of all laser-annealed ITO films.

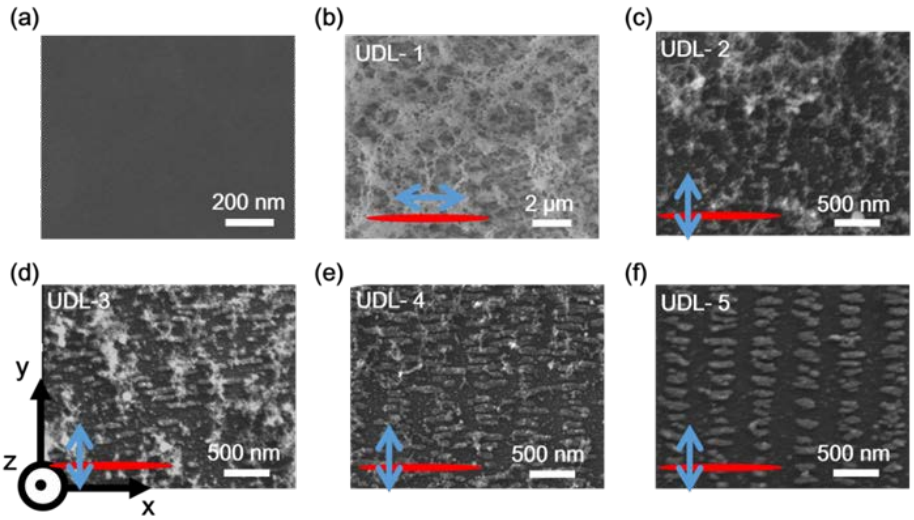

Fig. 1. SEM images showing the morphology of the ITO films before and after laser processing. (a) The surface morphology of an untreated ITO film. (b) A laser-annealed ITO film (UDL-1, fluence = 646 mJ/cm^2) with scanning along the y-axis and polarization (blue arrow) parallel to the laser line-spot (red). (c)–(f) Laser-annealed ITO films [UDL-2 (fluence = 217 mJ/cm^2), UDL-3 (fluence = 197 mJ/cm^2), UDL-4 (fluence = 68 mJ/cm^2) and UDL-5 (fluence = 60 mJ/cm^2)] with scanning along the y-axis and polarization (blue arrow) perpendicular to the laser line-spot (red)

For sample UDL-5, the nano-bricks with a length of ~250 nm (along the x-axis) and a width of ~70 nm (along the y-axis) are regularly separated by around 500 nm along the x-axis. This 500-nm-period structure, which is the so-called low spatial frequency LIPSS (LSFL) that is usually observed on the surface of dielectric materials, is parallel to the polarization of laser beam. When the photon energy is smaller than the bandgap of the material, the spatial period can be estimated by $\Lambda_{parallel} = \lambda/n$, where n is the refractive index of the dielectric material [9]. The spatial period, $\Lambda_{parallel} = \lambda/n$, which is attributed to radiation remnants, was already predicted by the LIPSS theory of Sipe *et al.* for transparent materials [17]. Radiation remnants could be generated at the solid/air interface by absorbing photons from the incident radiation and then transfer to the materials at the associated spatial frequencies. Additionally, electrons can be excited to higher energy levels by absorbing multiple photons when the photon energy is smaller than the bandgap of the material. In other words, the strong electric field of the laser drives the electrons to tunnel out and become the plasma, which further induces the ablation on surface of materials. The bandgap for ITO is around 3.7 eV [18] and the photon energy of the irradiated laser is 1.55 eV, so with a

Optics EXPRESS

refractive index n ~1.60 at 800 nm [19], it is estimated that $\Lambda_{parallel}$ = 500 nm, which is consistent with the experimental result for sample UDL-5.

Table 1. Laser fluence and the structure formation on the colorized ITO films.

Sample no.	Fluence (mJ/cm^2)	Nanostructure		Color
		cotton-like structure	brick-like structure	
UDL-1	646.1	V	–	Cyan
UDL-2	216.7	V	V	Yellow
UDL-3	197.0	V	V	Yellow
UDL-4	67.7	V	V	Orange
UDL-5	59.6	–	V	Orange

Interestingly, the colors of laser-annealed ITO films are controlled by varying the laser fluences, as shown in Fig. 2(a). The purple color of an untreated ITO film becomes cyan, yellow, or orange if there are different nanostructures on the surface of the laser-annealed ITO films. In order to clarify the origin of laser-colorized ITO films, the reflectance and transmittance spectra of all ITO films in the visible region were measured. Figure 2(b) shows the typical reflectance and transmittance spectra for an untreated ITO film with a relatively high reflectance at less than 425 nm and at more than 650 nm. Therefore, the untreated ITO film is purple. After laser processing, the reflectance spectra for the ITO films are significantly different. For high fluence (UDL-1), the reflectance spectrum from 450 to 600 nm is greater than that for an untreated ITO film, with a 2.2-fold increase at around 550 nm, but the reflectance spectra below 400 nm and above 650 nm shrink significantly. Therefore, the laser-colorized ITO film of UDL-1 is cyan. When the laser fluence decreases, the broad main peak in Fig. 2(c) gradually shifts from 550 nm to 575 nm and the color changes from cyan to the yellow and then orange.

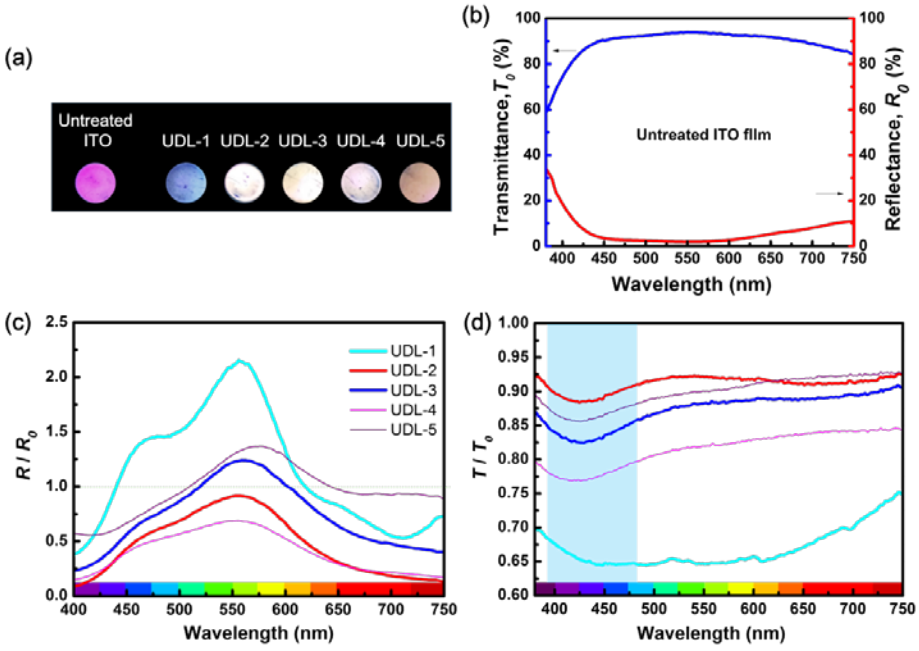

Fig. 2. (a) The colors of ITO films before and after laser processing. (b) The reflectance (R_0) and transmittance (T_0) spectra for an ITO film before laser processing. (c) The ratio of the reflectance spectra for the ITO films before (R_0) and after (R) laser processing. (d) The ratio of the transmittance spectra for the ITO films before (T_0) and after (T) laser processing. The blue shaded area covers the wavelengths that cause damage to eyes.

Optics EXPRESS

All of the transmittance spectra for ITO films are reduced after laser processing, as shown in Fig. 2(d). It is interesting to note that the reduction in the transmittance in the region from 390 nm to 480 nm [the blue area in Fig. 2(d)] is significantly greater than that in long-wavelength region. The region of 390-480 nm is dominated by blue light and has been demonstrated to cause damage to eyes [20]. The low fluence sample (UDL-5) gives a larger reduction in the blue-light region and a smaller reduction in the red-light region, so the femtosecond laser-colorized ITO films that are developed in this study can be directly used for LCD displays, because they maintain their original function as an electrode and act as a blue light filter to protect eyes.

When laser-colorized ITO films are used in the LCD displays, the image that is displayed on the LCD can be selectively screened by varying the view angle. Figure 3(a) shows the schematic for testing this concept. If the view angle θ is close to 0 (i.e., watching the panel normally), the image on the panel is shown in Fig. 3(b). However, if the view angle θ is significantly different to 0 (i.e., watching the panel obliquely), the image on the panel is blocked by the strong reflected light with colors that depend on θ [see Figs. 3(c)–3(e)]. Finally, the image on the panel cannot be seen. This shows the significant potential for applications that allow information security and the protection of privacy.

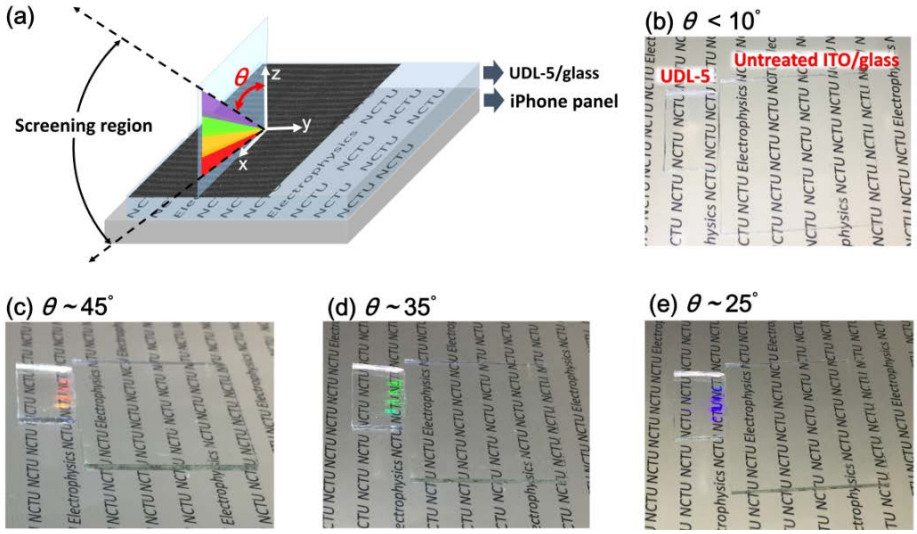

Fig. 3. (a) The schematic for capturing the images in (b)–(e), where θ is the view angle. (b)–(e) Observing the image on a screen through an untreated ITO film and a laser-colorized ITO film (UDL-5) at various view angles.

4. Conclusion

Cyan, yellow and orange laser-colorized ITO films are fabricated using femtosecond laser processing. For high laser fluences (>646 mJ/cm^2), a densely cotton-like structure is formed on the surface and there is a cyan color. For laser fluences of ~200 mJ/cm^2, both cotton-like and nano-bricks are simultaneously formed on the surface and a yellow color is produced. When the laser fluences are less than 68 mJ/cm^2, only a nano-brick structure is formed on the surface and an orange color is produced. The changes in the reflectance and transmittance spectra for ITO films that are annealed using a femtosecond laser are strongly dependent on the surface morphology, which also results in a change in color.

Previous studies have shown that femtosecond laser-induced nanostructures on ITO films enhance the conductivity [3,4], but also significantly modify the optical properties, as shown in this study. The significant reduction in transmittance in the blue-light region is good for eye protection. It is also demonstrated that laser-colorized ITO films with specific reflected

Optics EXPRESS

light can block the image behind the laser-colorized ITO film, which has potential application for information panels, in terms of information security and the protection of privacy.

Appendix

Crystal structure analysis

As shown in Fig. 4, the position and the full-width half-maximum (FWHM) of the peak (222) significantly changes after fs laser irradiation. By the well-known Scherrer formula [21], we further found that the average grain size of ITO thin films increases after fs laser irradiation. Consequently, the fs laser pulses indeed cause the changes of crystalline in ITO films.

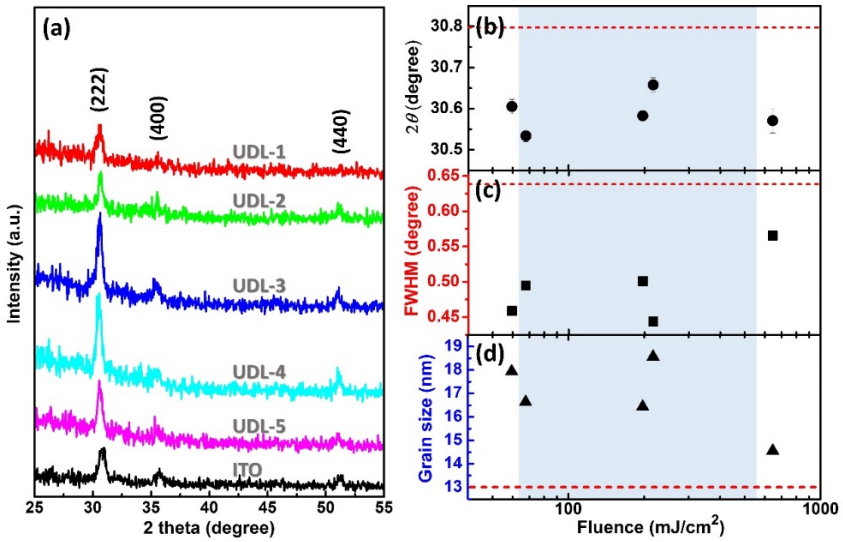

Fig. 4. (a) XRD patterns for untreated and laser treated ITO films (UDL-1, UDL-2, UDL-3, UDL-4 and UDL-5). (b) The fluence-dependent position of peak (222). (c) The fluence-dependent FWHM of peak (222). (d) The fluence-dependent grain size. (Red dash lines in (b)–(d) are the position, FWHM, and grain size of peak (222) in untreated ITO thin film, respectively.)

Electrical property and TEM/EDS images

We have performed the transport measurements to check the electrical properties of ITO films before and after fs laser irradiation. Figure 5 shows the laser fluence dependence of the resistance difference between an untreated ITO film and laser treated ITO films (UDL-1, UDL-2, UDL-3, UDL-4 and UDL-5). For example, the resistance difference between an untreated ITO film and the laser treated ITO film UDL-5 was estimated by

$$\Delta\Omega = \frac{\Omega_{UDL-5} - \Omega_0}{\Omega_0}. \quad (1)$$

Although the resistance of UDL-5 increased by 15% after laser processing, its resistivity may not increase due to the thickness shrinking of ITO films. For example, according to the inset of Fig. 6(a), the cross section area of UDL-5, $A_{\text{UDL-5}}$, is decreased by ~ 73% after laser processing. Because $\Omega_0 = 3.25\times10^6$ ohm, $\Omega_{\text{UDL-5}} = 3.75\times10^6$ ohm, and $A_{\text{UDL-5}} = 0.27A_0$, the resistivity can be expressed as

$$\rho_0 = \Omega_0 \times \frac{A_0}{L_0} = 3.25\times10^6 \times \frac{A_0}{L_0}, \quad (2)$$

Optics EXPRESS

$$\rho_{\mathrm{UDL-5}} = \Omega_{\mathrm{UDL-5}} \times \frac{0.27\,A_0}{L_0} = 3.75\times10^6 \times \frac{0.27\,A_0}{L_0}. \quad (3)$$

Assumed the thicknesses of all thin films are t_0 = 80 nm, we can further obtain

$$\frac{\rho_{UDL-5}}{\rho_0} = 0.31. \quad (4)$$

Therefore, the increase of resistance for laser treated ITO films is due to the shrink of thickness of ITO films. Actually, the resistivity of UDL-5 is decreased by ~70% after laser processing. Moreover, the Fig. 6(a) shows that the brick-like structure on UDL-5 is highly crystalline. The EDS mapping in Figs. 6(b)–6(e) also show that the rich-Sn and rich-In ITO films have been produced after laser processing. The metal-like clusters further lead to greater local conductivity [3]. Finally, we can conclude that the electrical properties of ITO films are not degraded after fs laser processing, even significantly improved.

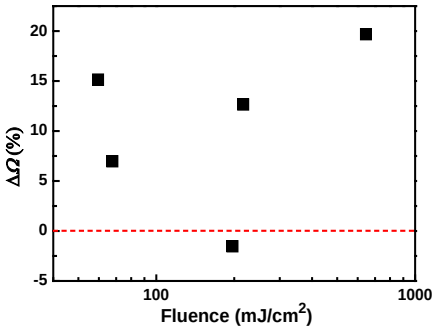

Fig. 5. Resistance difference between an untreated ITO film (Ω_0 = 3.25 × 10^6 ohm, probe distance = 1 mm, thickness = 80 nm) and laser treated ITO films (UDL-1, UDL-2, UDL-3, UDL-4 and UDL-5).

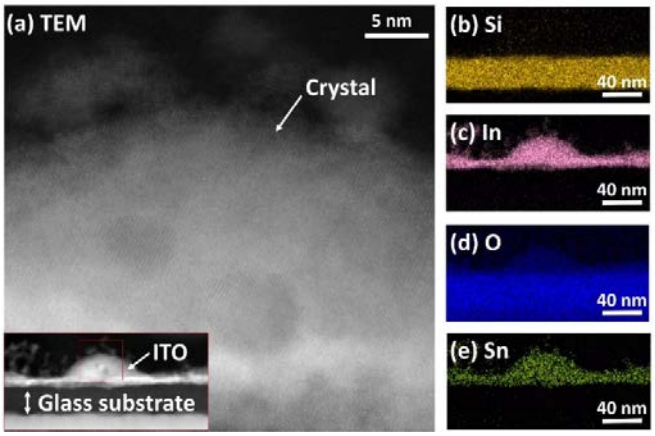

Fig. 6. (a) TEM image of the brick-like structure on UDL-5. Inset: TEM image of brick-like structure on UDL-5 corresponding to EDS mapping images in the (b)–(e), which characterize the silicon (Glass substrate), indium, oxygen and tin elements, respectively. (The TEM images and EDS analysis are provided by MSSCORPS CO.)

Absolute reflectance spectra

Figure 7 shows the absolute reflectance spectra for all ITO films prepared in this study. Generally, high transparency of ITO films (except UDL-1) results in the very low reflectance, which is hard to reveal the tiny changes of reflectance after laser processing. Therefore, the

Optics EXPRESS

R/R_0 spectra were applied to enhance the tiny changes of reflectance and help readers to recognize the significant changes of reflectance on ITO films after laser processing

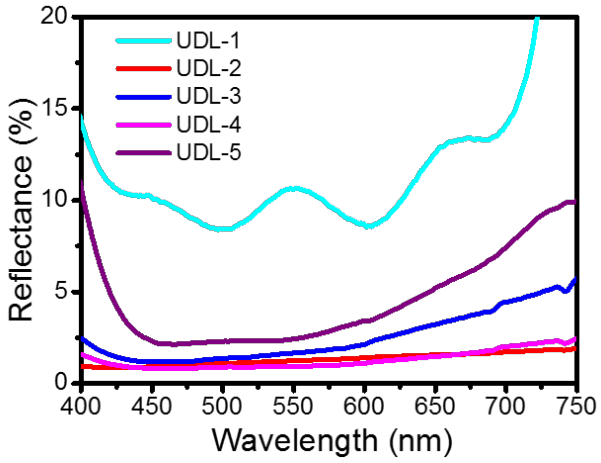

Fig. 7. The absolute reflectance spectra of all ITO films after laser processing.

Diffraction of the laser-printed ITO gratings

Due to the 500-nm-period pattern formed by the regular nano-bricks as shown in Fig. 8(a), UDL-5 exhibits different colors at specific viewing angles on the xz-plane. A white light source (i.e., a white light LED) was used to irradiate the sample with incident angle of θ_i =76°. Additionally, a spectrometer was also used to detect the diffraction spectra from θ_d = 90° to θ_d = 18° with the interval of 3° on the xz-plane. Figure 8(b) clearly shows that the diffraction wavelength shifts from 400 nm to 625 nm in the region of θ_d = 48° - 18°. At the larger angles (from θ_d = 81° to θ_d =51°), we can also observe the similar phenomenon. Meanwhile, the variation of dominant diffraction wavelengths at specific angles would cause the changes of colors on laser-treated ITO films. Consequently, the angle-dependent color of laser-colorized ITO films is definitely from the diffraction of the laser-printed ITO gratings.

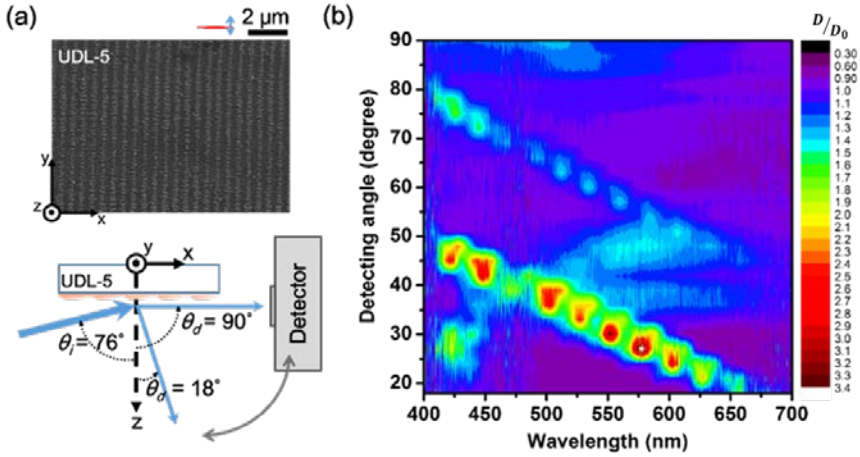

Fig. 8. (a) The schematics of angle-dependent (θ_d) diffraction spectrum measuring system and the surface morphology of a laser-annealed ITO film (UDL-5) used in this study. (b) The diffraction spectra as a function of diffraction angle (θ_d). D/D_0 is the diffraction intensity ratios between an untreated ITO film and a laser-annealed ITO film (UDL-5).

Optics EXPRESS

Acknowledgments

We would like to thank the staff of MSSCORPS CO. for their assistance in TEM specimen preparation and TEM/EDS analysis. This work is supported by the Ministry of Science and Technology of the Republic of China, Taiwan (Grant No's. 103-2923-M-009-001-MY3, 103-2628-M-00-002-MY3, 103-2119-M-009-004-MY3, 103-2119-M-009-007-MY3, 103-2112-M009-015-MY3 and 106-2628-M-009-003-MY3) and the Grant MOE ATU Program at NCTU.